Published in final edited form as:
Nucl Med Biol. 2007 November ; 34(8): 907–915.

In vivo dynamic imaging of myocardial cell death using ^{99m}Tc-labeled C2A domain of Synaptotagmin I in a rat model of ischemia and reperfusion

Zhonglin Liu[1], **Ming Zhao**[2], **Xiaoguang Zhu**[2], **Lars R. Furenlid**[1], **Yi-Chun Chen**[1], and **Harrison H. Barrett**[1]

1 *Department of Radiology, University of Arizona, Tucson, AZ*

2 *Department of Biophysics, Medical College of Wisconsin, Milwaukee, WI*

Abstract

This study was designed to investigate the capability of a small-animal SPECT imager, FastSPECT II, for dynamic rat heart imaging and to characterize the *in vivo* kinetic properties of ^{99m}Tc-C2A-GST, a molecular probe targeting apoptosis and necrosis, in detecting cell death in ischemic-reperfused rat hearts.

Methods—C2A-GST was radiolabeled with ^{99m}Tc via 2-iminothiolane thiolation. Myocardial ischemia-reperfusion was induced by 30-minute ligation of the left coronary artery followed by 120-minute reperfusion in seven rats. FastSPECT II cardiac images of ^{99m}Tc-C2A-GST in list-mode acquisition were recorded for 2 hours using FastSPECT II.

Results—Tomographic images showed a focal radioactive accumulation (hot spot) in the lateral and anterior walls of the left ventricle. The hot spot was initially visualized 10 minutes after injection and persisted on the 2-hour images. Quantitative analysis demonstrated that the hot spot radioactivity increased significantly within 30-minute post-injection and experienced no washout up to the end of the 2-hour study. The ratio of the hot spot/viable myocardium was 4.52 ± 0.24, and infarct-to-lung ratio was 8.22 ± 0.63 at 2 hours post-injection. The uptake of ^{99m}Tc-C2A-GST in the infarcted myocardium was confirmed by triphenyl tetrazolium chloride (TTC) staining and autoradiography analysis.

Conclusions—FastSPECT II allows quantitative dynamic imaging and functional determination of radiotracer kinetics in rat hearts. An *in vivo* kinetic profile of ^{99m}Tc-C2A-GST in the ischemic-reperfused rat heart model was characterized successfully. The pattern of accelerated ^{99m}Tc-C2A-GST uptake in the ischemic area-at-risk after reperfusion may be useful in detecting and quantifying ongoing myocardial cell loss induced by ischemia-reperfusion.

Keywords

Apoptosis; Necrosis; C2A; Heart; Rat; SPECT

For correspondence or reprints, contact: Zhonglin Liu, M.D., Department of Radiology, The University of Arizona, P.O. Box 245067, Tucson, AZ 85724-5067, Tel. 520-626-4248; Fax. 520-626-2892, E-mail: zliu@radiology.arizona.edu.

1. Introduction

Acute myocardial infarction (AMI) is characterized by extensive cardiac cell death in the ischemic area-at-risk (IAR). As major forms of cell death, apoptosis and necrosis take place in multiple types of cardiac cells and contribute significantly to the irreversible damage of the myocardium in ischemic-reperfused hearts [1–3]. The significance in identifying cell death and its pathways is that it can provide a novel therapeutic opportunity and lead to the design of a new class of therapeutic agents aimed at preventing cell death and lessening AMI. At least in theory, molecular imaging techniques that detect the molecular signatures of cell death can provide highly specific assessment of AMI. In practice, this can be accomplished using molecular probes, which recognize the molecular markers of cardiac cell death.

While apoptosis and necrosis are distinctly different modes of cell death, a common molecular marker, the exposure of anionic phospholipids (APLDs), allows their detection as a single comprehensive category in dead and dying tissues [4–6]. In normal cells, the APLDs, including phosphatidylserine (PtdS) and phosphatidylinositides (PtdIs), are strictly constituents of the inner leaflet of the plasma membrane. With the onset of apoptosis, PtdS is externalized and exposed onto the cell surface [6]. Since the redistribution of PtdS takes place in the execution phase of apoptosis and downstream of caspase activation, cells with externalized PtdS, which have already committed to the programmed cell death, are regarded as non-salvageable. In necrotic cells, the APLDs become accessible to the extracellular milieu as a passive consequence of compromised plasma membrane integrity. In essence, the exposure of APLDs embodies a common molecular marker for both apoptosis and necrosis. Being the major phospholipid components of the plasma membrane, once accessible, the APLDs provide abundant binding targets for detection.

APLD-binding proteins hold promise as molecular probes for the imaging of cell death, owing to their high affinity and specificity interactions with APLDs in membranes. To this end, derivatives of Annexin V in the detection of apoptosis in a wide range of model systems have been described [7–13]. The potential utilities of another protein, the C2A domain of Synaptotagmin I, have also been demonstrated [14–17]. Although both bind APLDs in a calcium-dependent fashion, Annexin V and C2A are rather structurally distinct proteins. In terms of binding activities, Annexin V binds PtdS almost exclusively, while C2A is more accommodative and interacts with PtdS and PtdIs with relatively high affinity.

C2A assay offers the possibility of detecting apoptosis and necrosis in vitro and *in vivo*. A fusion protein of C2A and glutathione-s-transferase (C2A-GST) can be radiolabeled with ^{99m}Tc and result in ^{99m}Tc-C2A-GST for *in vivo* scintigraphic imaging [16]. Potentially, ^{99m}Tc-C2A-GST imaging with SPECT will be one of the most sensitive methods for noninvasive detection of cardiac cell death. Using planar imaging, quantitative gamma counting, and autoradiography analysis, it has been demonstrated recently that ^{99m}Tc-C2A-GST accumulates avidly in the ischemic area-at-risk and binds predominantly to the infarcted myocardium [16,18]. When ^{99m}Tc-C2A-GST was injected 2 hours after reperfusion, it was retained in the infarcted tissues with little washout (less than 10%) for at least 24 hours [18]. However, this temporal uptake profile of ^{99m}Tc-C2A-GST in the infarcted myocardium was obtained by intravenously injecting ^{99m}Tc-C2A-GST at different time points after infarction (30-minute ischemia) and counting the tissue radioactivity using a gamma counter. The *in vivo* kinetic profile of ^{99m}Tc-C2A in myocardium with ischemia-reperfusion has not been clarified by imaging individual animals dynamically.

In order to quantify radiopharmaceutical kinetics *in vivo* in small animals, a high-resolution stationary SPECT system is essentially required. The Radiology Research Laboratory at the University of Arizona has designed and built a stationary small-animal SPECT imager, called

FastSPECT II, which consists of 16 modular cameras with a true-list-mode architecture acquiring SPECT projections simultaneously. Consequently, this study was designed to investigate the capability of the new stationary SPECT system for determining uptake and clearance kinetics of cardiovascular radiopharmaceuticals. Using FastSPECT II, we wanted to extend the existing finding and characterize the dynamic uptake profile of ^{99m}Tc-C2A-GST in a rat heart model with ischemia-reperfusion injury.

2. Materials and Methods

2.1. Radiopharmaceutical preparation

The fusion protein of C2A and glutathione-s-transferase (C2A-GST) was overexpressed in *E. Coli*, purified, and labeled with ^{99m}Tc, as previously described in detail [16]. Briefly, 200 μl of C2A-GST (2 mg/ml) was dissolved in PBS and incubated with 2 μl 2-iminothiolane (2-IT) (10 mg/ml in DMSO) at 37°C for 1 hour. Five hundred μl of $^{99m}TcO_4^-$ in 0.9% NaCl was added to a stannous glucoheptonate mixture (80 μg $SnCl_2$ versus 8 mg sodium glucoheptonate). Four hundred μl of ^{99m}Tc-glucoheptonate was then mixed with 200 μl of thiolated C2A-GST. The mixture was incubated at room temperature for 30 minutes, and the radiolabeled product was purified using Sephadex G-25 (column PD-10) pre-equilibrated with PBS, pH 7.4. The radiochemical purity (RCP) of ^{99m}Tc-C2A-GST was determined by instant thin-layer chromatography (ITLC-SG; Gelman Sciences) using 2 solvent systems as the mobile phase: saline and $NH_3.H_2O$/alcohol/H_2O (1:2:5). After gel-filtration purification, ^{99m}Tc-C2A-GST RCP was more than 98%. The stability of the labeled protein was greater than 96% in a 24-hour period in saline.

2.2. Ischemic-reperfused rat heart model preparation

Seven Sprague-Dawley rats (male, 250–300 g) were initially anesthetized with sodium pentobarbital (50 mg/kg) intraperitoneally. After intubation, respiration was maintained using a volume-controlled Inspira Advanced Safety Ventilator (Harvard Apparatus, Holliston, MA) with a mixture of oxygen and room air. The proximal left anterior descending coronary artery (LAD) was occluded for 30 minutes using a 6.0 Prolene suture at about 1 mm below the left atrial appendage. The onset of acute ischemia was confirmed by the pale appearance in the area-at-risk region immediately upon occlusion, and changes in ECG profiles, including the elevation of ST segment and a significant increase in the QRS complex amplitude and width. After reperfusion, the chest wall was closed in sutured layers, and ventilation was maintained until the rat could regain spontaneous respiration. The loose suture was left in place for ischemic area-at-risk staining.

2.3. Dynamic high-resolution SPECT imaging

The small-animal SPECT system, FastSPECT II, was built in the Radiology Research Laboratory at the University of Arizona. FastSPECT II employs 16 modular scintillation cameras, each with a NaI(Tl) scintillation crystal and 3 × 3 arrays of 1.5-inch-diameter PMTs [19]. Using a standard cylindrical aperture with 16 1-mm diameter pinholes in this study, the spatial resolution of this novel SPECT imager on reconstructed subjects is about 1.0 mm, and the system sensitivity is 10 cps/μCi. FastSPECT II provides dynamic imaging with a true-list-mode architecture. This powerful stationary SPECT system can digest 48 gigabits of raw information per second. FastSPECT II is capable of acquiring projection data without any motion of the object or detection system to produce excellent dynamic tomographic images.

The rat was anesthetized with 1.0%-1.5% isoflurane and placed inside the aperture using a translation stage. The animal was positioned so that the heart localized in the center of the field of view. At 120 minutes of reperfusion, ^{99m}Tc-C2A-GST (111–148 MBq, 0.5 ml) was injected intravenously via a pre-installed jugular vein catheter using a Harvard PHD2000 syringe pump

(Harvard Apparatus, Holliston, MA), followed by a 0.1-ml saline flush. Immediately after injection, dynamic cardiac images in list-mode acquisition were recorded over a 2-hour period using FastSPECT II. A total of 16 projections were obtained, one from each camera, to generate a data set for tomographic reconstruction.

2.4. Image processing

Tomographic reconstructions of FastSPECT II data were processed using 25 iterations of the OS-EM algorithm with 4 subsets, 4 projections per subset. Using AMIDE 0.8.7 software, 3D images were computed to provide images in a 41 × 41 × 41 voxel format. The oblique re-orientation of transaxial data was performed by computerized procedures to generate tomographic short-axis (transverse), coronal, and sagittal slices with one-voxel thickness (1.0 mm).

For each rat, a 3D region-of-interest (ROI) analysis was applied to generate myocardial time-activity curves (TACs). ROIs around the "hot-spot" radioactive accumulations of ^{99m}Tc-C2A-GST on the 120-minute images were created on all transverse slices from the base to the apex, which could be viewed simultaneously on the coronal and sagittal slices. The 120-minute ROIs were applied to all of the dynamic images from 1 to 120 minutes for determining averaged hot spot TACs, which were corrected for ROI size (pixels), radioactive decay, and acquisition time. The remote normal myocardial TACs were generated using similar ROI analysis. Care was taken to draw an ROI on the normal zone and avoid the overlapping of the ROI into the blood pool on the early time-point images. To do that, the tomographic 1-minute cardiac blood pool images were co-registered with 120-minute images to ensure the ROI establishment off the left ventricular cavity.

Based on the time-activity curves, the averaged fractional washout and retention at each time-point image relative to the initial radioactivity on the 1-minute image and 10-minute image, as well as the ratios of hot spot activities to remote normal myocardial activities, were calculated subsequently.

2.5. Histological and autoradiograph analysis

To confirm the distribution of ^{99m}Tc-C2A-GST in cardiac tissues, each rat was sacrificed by intraperitoneal injection of an overdose of sodium pentobarbital (200 mg/kg). After thoracotomy, the heart was excised and rinsed with cold saline solution. Two ml of pre-warmed TTC solution (2.5% in PBS, w/v, pH 7.4) were perfused in retrograde manner into the entire myocardium via the aorta within one minute. The heart was incubated with TTC solution for 15 minutes at 37°C, and then was subsequently fixed in 10% PBS-buffered formalin overnight at 2–8°C to terminate TTC reduction reaction and to preserve the tissue morphology. The fixed heart was sliced into consecutive slices of 0.5 mm each. The TTC-stained tissue sections were photographed using a digital photodocumentation camera.

The spatial distribution of radioactivity was examined using autoradiography. The tissue slices were covered with 1 layer of plastic wrap and exposed to the FujiFilm phosphor imaging plates for 5–15 minutes. A FujiFilm BAS5000 Bio-Imaging Analysis System (Stamford, CT) was used to scan the plates for digital autoradiograph collection.

2.6. Data analysis

All quantitative results were expressed as mean ± S.E.M. Comparisons between two variables were assessed performed with one-way analysis of variance. Probability values less than 0.05 were considered significant.

2.7. Ethics

The animal experiments were performed in accordance with the Principles of Laboratory Animal Care from the National Institutes of Health (NIH Publication 85–23, revised 1985) and were approved by the Institutional Animal Care and Use Committee (IACUC) at the University of Arizona.

3. Results

3.1. FastSPECT II images of myocardium with ischemia-reperfusion

The *in vivo* uptake profile of ^{99m}Tc-C2A-GST in the infarcted hearts was depicted in dynamic tomographic images. As shown in Figure 1, blood-pool signals were seen at the time of tracer injection on the 1-minute image. Then, the wall of the left ventricle was partly visualized in the stenosis zone, which exhibited a distinct focal radioactive accumulation (hot spot) in the lateral and anterior walls of the left ventricle. By 10–30 minutes post-injection, the hot spot has become apparent. The spatial distribution of focal radioactivity uptake remains persistent over time, while becoming increasingly prominent over the 2-hour post-injection period, presumably due to a receding blood-pool background and/or continuous uptake of ^{99m}Tc-C2A-GST. The overall distribution of ^{99m}Tc-C2A-GST in the chest and upper abdomen at 120 minutes post-injection is shown in Figure 2. High radioactive uptake in the liver was observed on the tomographic coronal and sagittal slices of FastSPECT II images with ^{99m}Tc-C2A-GST. The most prominent radioactive uptake in the chest was found on the anterior wall, lateral wall, and apex of the left ventricle, which corresponded to the ischemic area-at-risk of the LAD-supplied area. In all of the animals with myocardial ischemia-reperfusion, FastSPECT II tomographic images depicted well-defined hot spot uptake. The presence of radioactivity in the lungs was low.

3.2. Quantitative analysis of ^{99m}Tc-C2A-GST imaging

Myocardial TACs were generated using computerized ROI analysis with background, decay, and acquisition time correction. Tracer kinetics of ^{99m}Tc-C2A-GST is summarized in Figure 3. The difference observed at each point in time from 5 minutes to 120 minutes between the LCA hot spot and normal zone was significant. The difference between the LCA hot spot and lung started from 10 and 15 minutes. The time-dependent plots indicate that essentially no washout took place in the ischemic-reperfused myocardium during the 2-hour acquisition period. Instead, an increased uptake pattern of ^{99m}Tc-C2A-GST was observed in the infarcted zone, where the radioactivity was markedly accelerated within the first 30-minute post-injection, and then slowly increased until 120 minutes post-injection.

When the hot spot radioactivity at the 120-minute image was normalized to the initial peak activity at 1 minute post-injection, the fractional retention (%) of ^{99m}Tc-C2A-GST from the hot spot was significantly higher than that from the remote viable zone in all hearts (167.2 ± 12.8 vs. 46.6 ± 10.8, $P < 0.01$). The radioactivity at the 120-minute point was furthermore normalized by the activity at 10 minutes to calculate the percentage of radioactive retention. The fractional retention (% 10-minute peak) in the hot spot at the conclusion of imaging was still higher than that in the normal zone in all hearts (150.3 ± 7.6 vs. 51.5 ± 7.6, $P < 0.01$). Relative to the normal myocardium, in which ^{99m}Tc-C2A-GST radioactivity exhibited lower than initial level, the ischemic area-at-risk (hot spot) at the end of imaging session showed 50.3% extra accumulation compared to the radioactive level at 10-minute post-injection.

Figure 4 shows that the ratios of the hot-spot/normal myocardium and the hot-spot/lung activity increased with time following ^{99m}Tc-C2A-GST administration. At 2 hours after injection, the average ratio of hot spot to remote viable myocardium was 4.52 ± 0.24 (max: 15.4 ± 2.0; min: 1.13 ± 0.06), and the infarct-to-lung ratio was 8.22 ± 0.63.

3.3. Histological and autoradiograph analysis

Myocardial infarction in the ischemic-reperfused hearts was confirmed by postmortem triphenyl tetrazolium chloride (TTC) staining. The infarct size (% left ventricle) quantified by SigmaScan analysis was 25.3 ± 3.7. As shown in Figure 5, tracer uptake in tissue sections consistently co-localized with TTC-deficient infarcted regions. Within the infarcted myocardium, the distribution of radioactivity appears to be prominent and heterogeneous. According to semi-quantitative autoradiography, at 2-hour post-injection, the level of radioactivity in the infarcted myocardium was significantly higher than that in the remote normal myocardium. The average ratio of infarct/normal myocardium was 10.7 ± 0.9 with a range from 5.2 to 22.7.

4. Discussion

Myocardial cell death during ischemia-reperfusion can take place via apoptosis and necrosis. The individual contributions of these two phenomena, and at what point they contribute to tissue death, are unclear. It is believed that necrotic myocytes may also undergo early changes of apoptosis [20] or share common molecular pathways [1,21–23]. Clinically, there is a need for new methods to gain more understanding of the role of necrosis and apoptosis in the ischemic-reperfused heart and assess therapeutic interventions aimed at decreasing myocytic damage. A useful technique would be one that identifies not only the presence of damage, but also its site and extent, to permit a stratified approach to therapy.

One of the merits in the current study is the exciting use of the newly designed small-animal SPECT system, FastSPECT II. This dynamic SPECT imager has 16 cameras acquiring SPECT projections simultaneously with a true-list-mode architecture [19]. The front-end “list-mode event processors” can examine incoming digitized data streams for valid events and package up the measurements associated with an event in a byte packet, i.e., a list-mode data entry. PCI-bus back-end boards accumulate the data, which include the time of each event to the nearest 30 nanosecond clock tick and append each valid event packet as it arrives from a front end to the appropriate list. In addition, FastSPECT II has more flexibility in choosing magnification, resolution, and field-of-view than the original FastSPECT design. As demonstrated in the current study, FastSPECT II produces excellent static and dynamic images with quantitative analysis capabilities to facilitate the characterization of the real-time uptake profile of ^{99m}Tc-C2A-GST along with the evolving myocardial damage.

The dynamic images of ^{99m}Tc-C2A-GST acquired by FastSPECT II consistently reflected the location and extent of irreversible myocardial damage in the ischemic-reperfused rat heart model. The high affinity of ^{99m}Tc-C2A-GST to APLDs in the ischemically injured myocardium made the infarction visualizable about 30 minutes after intravenous administration. The focal uptake of radioactivity results in a prominent hot spot, which co-registers with the infarcted myocardium. The radioactivity level remained persistent for an extended period of time without washout. The infarct was well-defined for at least 120 minutes following injection. The location of infarction and distribution of ^{99m}Tc-C2A-GST were consequently confirmed by biochemical assay and autoradiograph analysis.

Quantitative analyses on dynamic FastSPECT II images with ^{99m}Tc-C2A-GST made it possible to identify the progression of myocardial injury induced by ischemia-reperfusion. The appearance of ^{99m}Tc-C2A-GST time-activity curves showed a rapid early clearance phase followed by a slow second phase in the normal myocardium and lungs. The occurrence of myocardial ischemia-reperfusion injury altered the kinetic profile of ^{99m}Tc-C2A-GST in the necrotic myocardium and produced an increased uptake pattern of ^{99m}Tc-C2A-GST. The kinetic uptake of ^{99m}Tc-C2A-GST was markedly accelerated within the first 30-minute post-injection. Beginning at 15 minutes after injection, the radioactivity in the infarcted myocardium

reached a statistically higher level than that initial 1 minute after injection. This observation cannot be explained completely by the receded blood pool background. Most likely, the continuously increasing uptake of ^{99m}Tc-C2A-GST was due to the ongoing myocytic apoptosis in the reperfusion phase, which is a gradual and continuous process. Myocardial apoptosis is primarily triggered or accelerated during reperfusion and acts as a crucial pathway in expansion of injury. When reperfusion of the ischemic area begins, apoptotic cell death occurs during both the early and late phases of reperfusion from hours to days [24,25]. Based on our knowledge, the finding regarding the continuously increased uptake of ^{99m}Tc-C2A-GST in the ischemic-reperfused myocardium is the first imaging demonstration of the *in vivo* ongoing myocardial damage noninvasively and dynamically. Thus, dynamic ^{99m}Tc-C2A-GST SPECT imaging with quantitative analysis may allow interrogation of the ischemic-reperfused myocardium undergoing apoptosis pathway at different phases and thereby permit detection and treatment of injuries before the onset of severe cardiac functional failure.

Several categories of molecular probes have been applied experimentally and clinically for imaging detection of myocardial cell death [26]. Although a direct comparison between ^{99m}Tc-C2A-GST and other probes is beyond the objective of this study, the difference of ^{99m}Tc-C2A-GST and ^{99m}Tc-glucarate kinetic profiles obtained from dynamic SPECT imaging in our laboratory using similar ischemic-reperfused rat heart models provides a good example to demonstrate the important role of a stationary SPECT system in preclinical investigation of cardiovascular radiopharmaceuticals. ^{99m}Tc-glucarate can mark acute necrotic cells, but does not localize in acute myocardial apoptosis [27]. We previously characterized *in vivo* radiopharmaceutical kinetics of ^{99m}Tc-glucarate and found that ^{99m}Tc-glucarate exhibited biphasic washout from the LCA ischemic-reperfused area and normal myocardial zone [28]. The early phase showed fast washout, and the late phase showed slow washout. The kinetic analysis indicates that ^{99m}Tc-glucarate may not provide the information regarding the ongoing myocytic injury during reperfusion, which is primarily accelerated in a time-dependent manner through apoptosis. In contrast, ^{99m}Tc-C2A-GST exhibited biphasic continuous uptake and experienced no washout up to the end of the 2-hour study. The radioactive uptake reached a plateau within 30 minutes after radiotracer injection, followed by a relatively slower increasing tendency. The quantitative analysis of radioactive hot spot accumulation in the ischemic-reperfused myocardium reveals the characteristic difference between ^{99m}Tc-C2A-GST and ^{99m}Tc-glucarate in specific detection of myocytic cell death.

The pathophysiological changes in the ischemic-reperfused myocardium induce not only various forms of cell death, but also exacerbate vascular permeability and increase interstitial space [29]. As a result, the radioactivity detected in the ischemic-reperfused myocardium in the present study might be a combination of specific APLD binding and nonspecific leakage of the tracer. Studies by Zhao and associates have shown that the passive distribution due to elevated vascular permeability was diminished from continuous washout [16]. The accelerated kinetic uptake of ^{99m}Tc-C2A-GST observed in the ischemic-reperfused myocardium thereby reflects the prominent specific binding of the molecular probe. Thus, ^{99m}Tc-C2A-GST uptake determined by dynamic SPECT imaging indicated that there were continuous myocytic injuries in the rat heart model, whereas passive leakage alone was insufficient for such observation.

Using a γ-camera with parallel-hole collimator, ^{99m}Tc-C2A-GST *in vivo* planar imaging of AMI in rats was described previously [16]. The images were obtained at a single time point. Although a hot spot uptake was visible as early as 40 minutes after injection on the planar images, the quantitative analysis of *in vivo* ^{99m}Tc-C2A-GST kinetics was hindered in the rat heart models because of poor temporal and spatial resolution of the planar camera. In order to determine washout rates and other kinetic parameters of radiolabeled agents using small-animal models, the temporal resolution of a small-animal SPECT system needs to be high to extract accurate estimates of these parameters. In our rat heart models of the present study, dynamic

cardiac images were obtained in list-mode acquisition with FastSPECT II. The myocardial radioactivities in the ischemic-reperfused zone and remote viable zone could be quantified accurately, and the uptake kinetics of ^{99m}Tc-C2A-GST was determined effectively. The pattern of kinetic profile in infarcted myocardium determined by FastSPECT II imaging was similar to that obtained by sacrificing animals at different time points after intravenous injection of ^{99m}Tc-C2A-GST and measuring tissue radioactivites using γ-counting [18].

5. Conclusion

FastSPECT II allows quantitative dynamic imaging and functional determination of radiotracer kinetics in rat hearts. Using dynamic FastSPECT II imaging, an *in vivo* kinetic profile of ^{99m}Tc-C2A-GST in the rat heart model with ischemia-reperfusion injury was characterized successfully. The pattern of accelerated ^{99m}Tc-C2A-GST uptake in the ischemic area-at-risk after reperfusion may be clinically useful in detecting and quantifying ongoing myocardial cell loss induced by ischemia-reperfusion.

Acknowledgements

The authors wish to acknowledge the technical support of Christy Barber and the editorial assistance of Corrie Thies. This work was supported by NIH grant P41 EB002035 and an American Heart Association grant.

References

1. Gottlieb RA, Engler RL. Apoptosis in myocardial ischemia-reperfusion. Ann N Y Acad Sci 1999;874:412–6. [PubMed: 10415551]
2. Majno G, Joris I. Apoptosis, oncosis, and necrosis. An overview of cell death. Am J Pathol 1995;146:3–15. [PubMed: 7856735]
3. Buja LM, Entman ML. Modes of myocardial cell injury and cell death in ischemic heart disease. Circulation 1998;98:1355–7. [PubMed: 9760287]
4. Martin SJ, Reutelingsperger CP, McGahon AJ, Rader JA, van Schie RC, LaFace DM, et al. Early redistribution of plasma membrane phosphatidylserine is a general feature of apoptosis regardless of the initiating stimulus: inhibition by overexpression of Bcl-2 and Abl. J Exp Med 1995;182:1545–56. [PubMed: 7595224]
5. Verhoven B, Schlegel RA, Williamson P. Mechanisms of phosphatidylserine exposure, a phagocyte recognition signal, on apoptotic T lymphocytes. J Exp Med 1995;182:1597–601. [PubMed: 7595231]
6. van Heerde WL, Robert-Offerman S, Dumont E, Hofstra L, Doevendans PA, Smits JF, et al. Markers of apoptosis in cardiovascular tissues: focus on Annexin V. Cardiovasc Res 2000;45:549–59. [PubMed: 10728376]
7. Tait JF, Gibson D. Measurement of membrane phospholipid asymmetry in normal and sickle-cell erythrocytes by means of annexin V binding. J Lab Clin Med 1994;123:741–8. [PubMed: 8195679]
8. Tait JF, Cerqueira MD, Dewhurst TA, Fujikawa K, Ritchie JL, Stratton JR. Evaluation of annexin V as a platelet-directed thrombus targeting agent. Thromb Res 1994;75:491–501. [PubMed: 7992250]
9. Blankenberg FG, Katsikis PD, Tait JF, Davis RE, Naumovski L, Ohtsuki K, et al. Imaging of apoptosis (programmed cell death) with ^{99m}Tc annexin V. J Nucl Med 1999;40:184–91. [PubMed: 9935075]
10. Blankenberg FG, Katsikis PD, Tait JF, Davis RE, Naumovski L, Ohtsuki K, et al. *In vivo* detection and imaging of phosphatidylserine expression during programmed cell death. Proc Natl Acad Sci U S A 1998;95:6349–54. [PubMed: 9600968]
11. Kietselaer BL, Reutelingsperger CP, Boersma HH, Heidendal GA, Liem IH, Crijns HJ, et al. Noninvasive detection of programmed cell loss with ^{99m}Tc-labeled annexin A5 in heart failure. J Nucl Med 2007;48:562–7. [PubMed: 17401092]
12. Sarda-Mantel L, Michel JB, Rouzet F, Martet G, Louedec L, Vanderheyden JL, et al. (99m)Tc-annexin V and (111)In-antimyosin antibody uptake in experimental myocardial infarction in rats. Eur J Nucl Med Mol Imaging 2006;33:239–45. [PubMed: 16283183]

13. Mukherjee A, Kothari K, Toth G, Szemenyei E, Sarma HD, Kornyei J, et al. ^{99m}Tc-labeled annexin V fragments: a potential SPECT radiopharmaceutical for imaging cell death. Nucl Med Biol 2006;33:635–43. [PubMed: 16843838]
14. Jung HI, Kettunen MI, Davletov B, Brindle KM. Detection of apoptosis using the C2A domain of synaptotagmin I. Bioconjug Chem 2004;15:983–7. [PubMed: 15366950]
15. Neves AA, Krishnan AS, Kettunen MI, Hu DE, Backer MM, Davletov B, Brindle KM. A Paramagnetic Nanoprobe To Detect Tumor Cell Death Using Magnetic Resonance Imaging. Nano Lett 2007;7:1419–23. [PubMed: 17411099]
16. Zhao M, Zhu X, Ji S, Zhou J, Ozker KS, Fang W, et al. ^{99m}Tc-labeled C2A domain of synaptotagmin I as a target-specific molecular probe for noninvasive imaging of acute myocardial infarction. J Nucl Med 2006;47:1367–74. [PubMed: 16883018]
17. Zhao M, Beauregard DA, Loizou L, Davletov B, Brindle KM. Non-invasive detection of apoptosis using magnetic resonance imaging and a targeted contrast agent. Nat Med 2001;7:1241–4. [PubMed: 11689890]
18. Zhu X, Li Z, Zhao M. Imaging Acute Cardiac Cell Death: Temporal and Spatial Distribution of ^{99m}Tc-Labeled C2A in the Area at Risk After Myocardial Ischemia and Reperfusion. J Nucl Med 2007;48:1031–6. [PubMed: 17536109]
19. Furenlid LRWD, Chen YC, Kim H, Pietraski PJ, Crawford MJ, Barrett HH. FastSPECT II: a second-generation high-resolution dynamic SPECT imager. IEEE Trans Nucl Sci 2004;51:631–5.
20. Aikawa R, Komuro I, Yamazaki T, Zou Y, Kudoh S, Tanaka M, et al. Oxidative stress activates extracellular signal-regulated kinases through Src and Ras in cultured cardiac myocytes of neonatal rats. J Clin Invest 1997;100:1813–21. [PubMed: 9312182]
21. Gill C, Mestril R, Samali A. Losing heart: the role of apoptosis in heart disease--a novel therapeutic target? Faseb J 2002;16:135–46. [PubMed: 11818361]
22. Otani H, Uchiyama T, Yamamura T, Nakao Y, Hattori R, Ninomiya H, et al. Effects of the Na+/H+ exchange inhibitor cariporide (HOE 642) on cardiac function and cardiomyocyte cell death in rat ischaemic-reperfused heart. Clin Exp Pharmacol Physiol 2000;27:387–93. [PubMed: 10831241]
23. Shimizu S, Eguchi Y, Kamiike W, Waguri S, Uchiyama Y, Matsuda H, et al. Retardation of chemical hypoxia-induced necrotic cell death by Bcl-2 and ICE inhibitors: possible involvement of common mediators in apoptotic and necrotic signal transductions. Oncogene 1996;12:2045–50. [PubMed: 8668329]
24. Zhao ZQ, Velez DA, Wang NP, Hewan-Lowe KO, Nakamura M, Guyton RA, et al. Progressively developed myocardial apoptotic cell death during late phase of reperfusion. Apoptosis 2001;6:279–90. [PubMed: 11445670]
25. Blancke F, Claeys MJ, Jorens P, Vermeiren G, Bosmans J, Wuyts FL, et al. Systemic inflammation and reperfusion injury in patients with acute myocardial infarction. Mediators Inflamm 2005;2005:385–9. [PubMed: 16489260]
26. Khaw BA. The current role of infarct avid imaging. Semin Nucl Med 1999;29:259–70. [PubMed: 10433340]
27. Khaw BA, Nakazawa A, O'Donnell SM, Pak KY, Narula J. Avidity of technetium 99m glucarate for the necrotic myocardium: in vivo and in vitro assessment. J Nucl Cardiol 1997;4:283–90. [PubMed: 9278874]
28. Liu Z, Barrett HH, Stevenson GD, Kastis GA, Bettan M, Furenlid LR, et al. High-resolution imaging with (99m)Tc-glucarate for assessing myocardial injury in rat heart models exposed to different durations of ischemia with reperfusion. J Nucl Med 2004;45:1251–9. [PubMed: 15235074]
29. Saeed M, van Dijke CF, Mann JS, Wendland MF, Rosenau W, Higgins CB, et al. Histologic confirmation of microvascular hyperpermeability to macromolecular MR contrast medium in reperfused myocardial infarction. J Magn Reson Imaging 1998;8:561–7. [PubMed: 9626869]

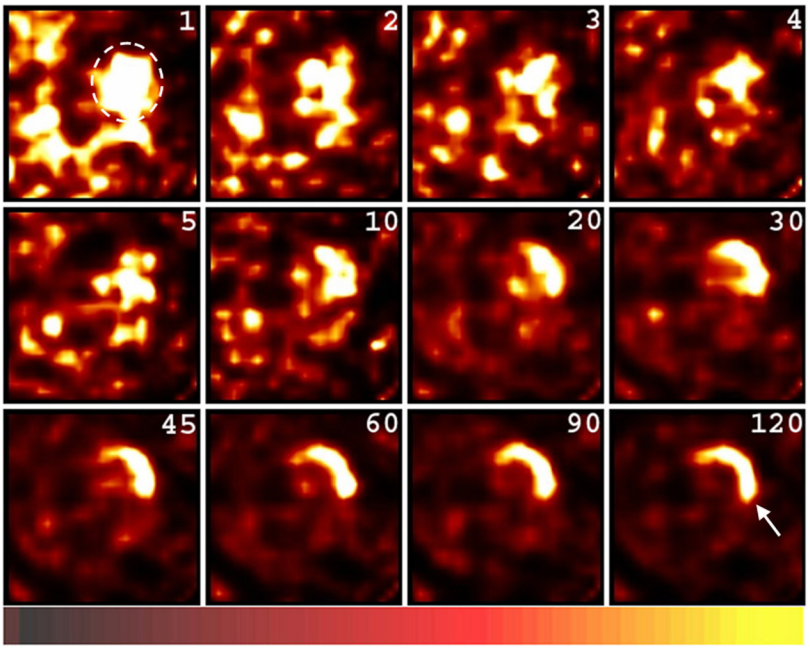

Figure 1.

Representative dynamic tomographic images of ^{99m}Tc-C2A-GST using a series of the same transaxial slice at each time point in a rat heart with ischemia-reperfusion (injected dose = 3.4 mCi). The rat was anesthetized with 1.2% isoflurane. The number in the upper right corner represents the post-injection time. The integrated images were parsed and split into dynamic 1-minute images. The cardiac blood pool (dashed mark) is evident on the 1-minute image. A good infarct definition with a regional hot spot in the left ventricular wall was achieved 10–30 minutes after radiotracer administration. The hot spot becomes increasingly prominent in size and radioactivity from 10 to 120 minutes post-injection. The arrow on 120-minute indicates the site of the infarct.

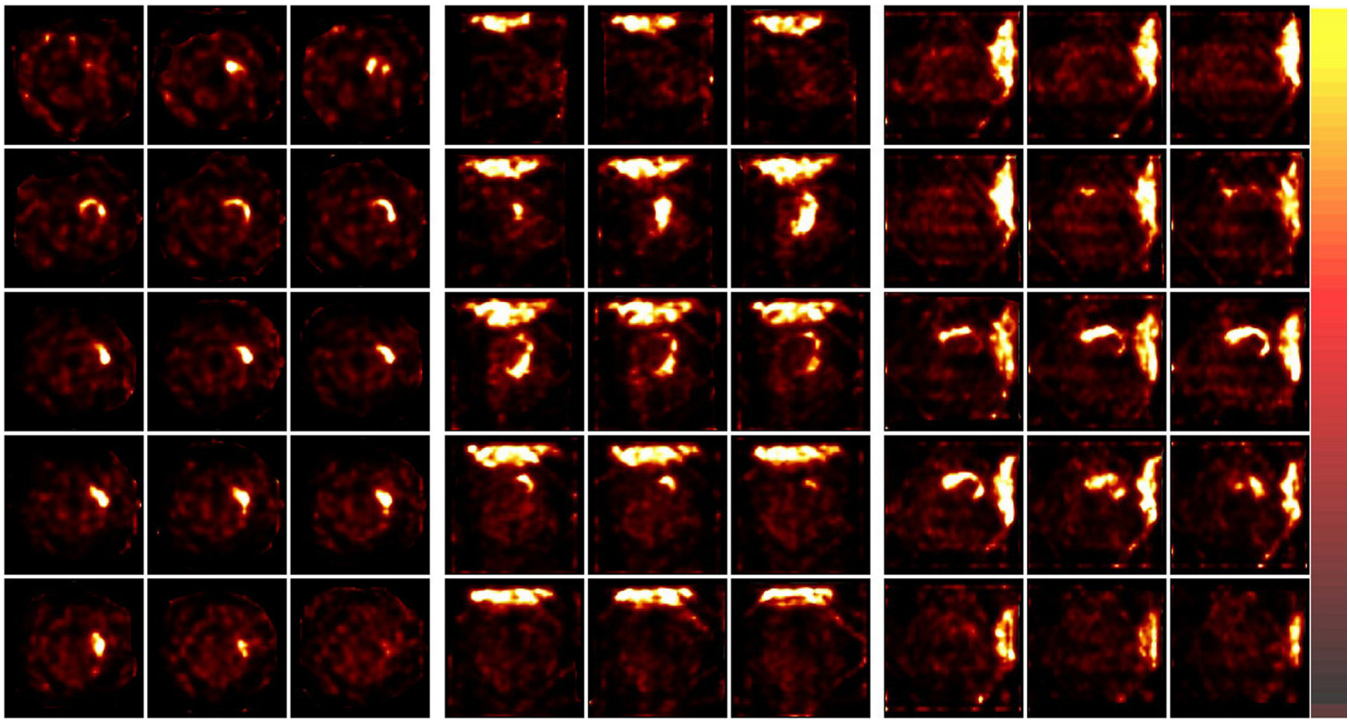

Figure 2.
Representative FastSPECT II transversal (left), coronal (middle), and sagittal (right) tomographic slices 2 hours post-injection of ^{99m}Tc-C2A-GST in a rat heart with myocardial infarction (injected dose = 3.4 mCi, 5-minute acquisition). The rat was anesthetized with 1.2% isoflurane. ^{99m}Tc-C2A-GST "hot spot" accumulations localized in the lateral wall, anterior wall, and apex of the left ventricle. The radioactive distribution of the remote normal myocardium and the lungs was low. The prominent liver uptake of ^{99m}Tc-C2A-GST was observed on the coronal and sagittal slices.

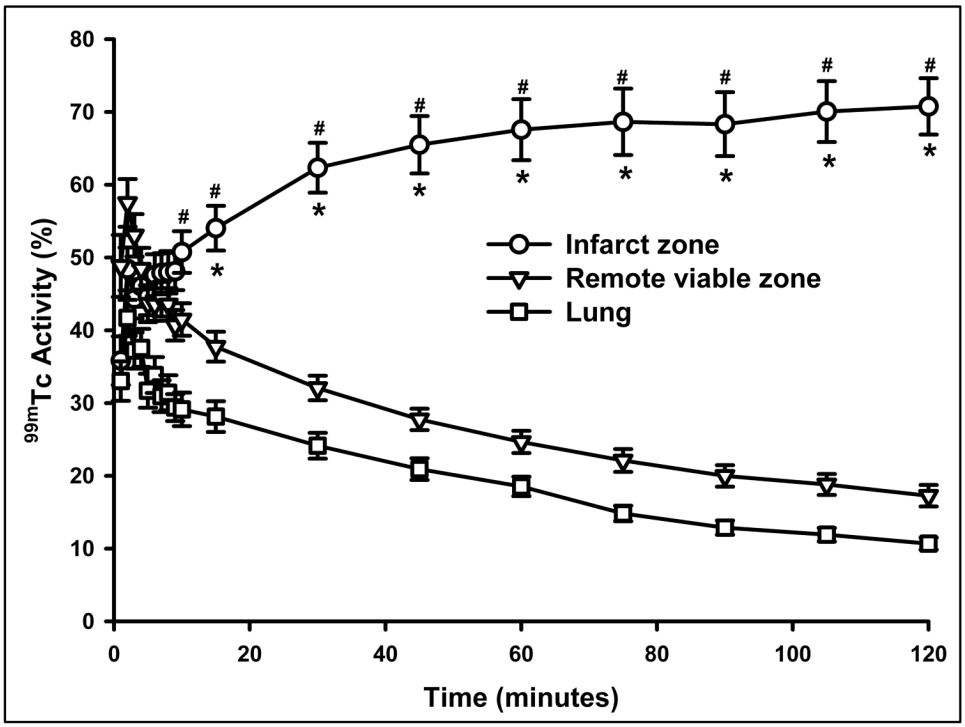

Figure 3.
^{99m}Tc-C2A-GST time-activity curves from infarcted myocardium, remote viable zone, and lungs in the rat hearts with ischemia-reperfusion injury. The curves were corrected by decay and acquisition time. * = $P < 0.05$ compared to remote viable zone, # = $P < 0.05$ compared to lung.

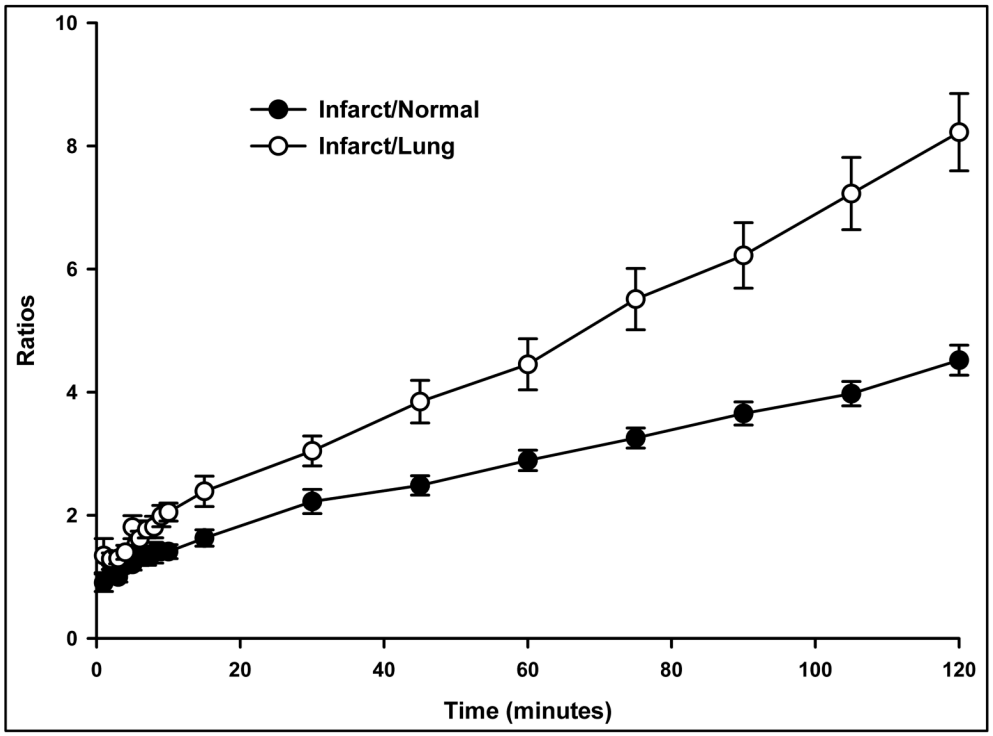

Figure 4.
Ratios of the infarct/normal myocardium and the infarct/lung activity increased with time following ^{99m}Tc-C2A-GST administration in the ischemic-reperfused rat hearts.

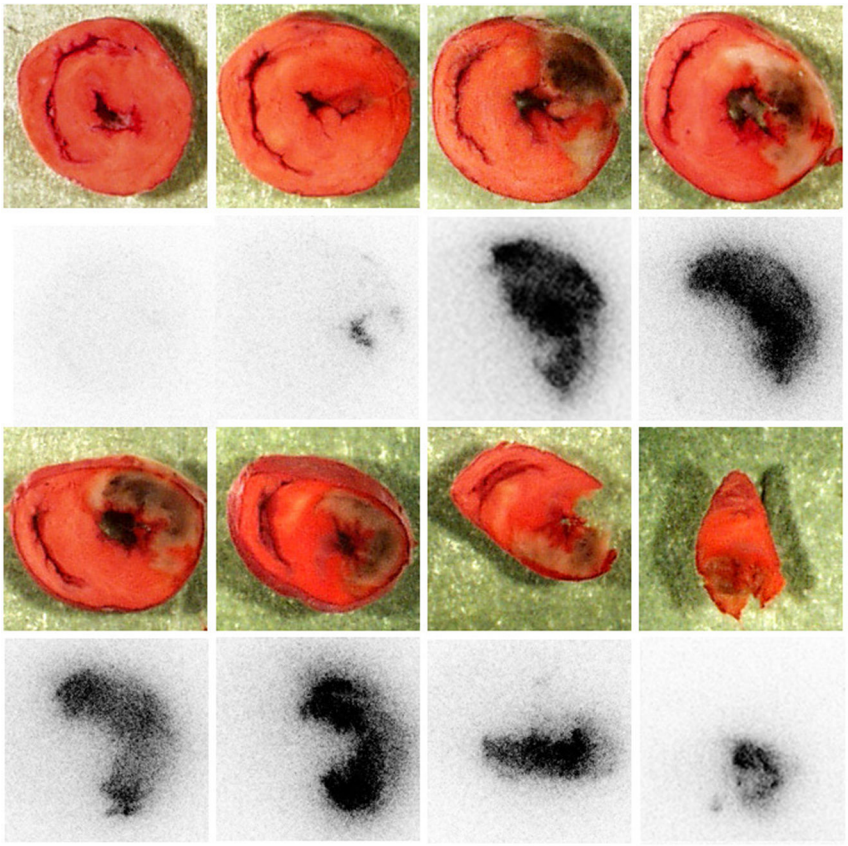

Figure 5.
Photographs of TTC staining (first and third row) and autoradiograph images (second and fourth row) from a representative ischemic-reperfused rat heart. The location and size of myocardial infarction (negative TTC staining) were consistent with the positive accumulation of ^{99m}Tc-C2A-GST determined by autoradiograph imaging.